

Adaptive Patch Contrast for Weakly Supervised Semantic Segmentation

Wangyu Wu^{a,b}, Tianhong Dai^c, Zhenhong Chen^e, Xiaowei Huang^b, Jimin Xiao^a,
Fei Ma^{a,*}, Renrong Ouyang^{d,*}

^a*Xi'an Jiaotong-Liverpool University, Suzhou, China*

^b*University of Liverpool, Liverpool, UK*

^c*University of Aberdeen, Aberdeen, UK*

^d*Suzhou Construction and Transportation Branch, Jiangsu United Vocational and Technical College, Suzhou, China*

^e*Microsoft, Redmond, USA*

Abstract

Weakly Supervised Semantic Segmentation (WSSS), using only image-level labels, has garnered significant attention due to its cost-effectiveness. Typically, the framework involves using image-level labels as training data to generate pixel-level pseudo-labels with refinements. Recently, methods based on Vision Transformers (ViT) have demonstrated superior capabilities in generating reliable pseudo-labels, particularly in recognizing complete object regions. However, current ViT-based approaches have some limitations in the use of patch embeddings, being prone to being dominated by certain abnormal patches, as well as many multi-stage methods being time-consuming and lengthy in training, thus lacking efficiency. Therefore, in this paper, we introduce a novel ViT-based WSSS method named *Adaptive Patch Contrast* (APC) that significantly enhances patch embedding learning for improved segmentation effectiveness. APC utilizes an Adaptive-K Pooling (AKP) layer to address the limitations of previous max pooling selection methods. Additionally, we propose a Patch Contrastive Learning (PCL) to enhance patch embeddings, thereby further improving the final results. We

*Corresponding authors

Email addresses: wangyu.wu22@student.xjtlu.edu.cn (Wangyu Wu),
tianhongdai914@gmail.com (Tianhong Dai), zcheh@microsoft.com (Zhenhong Chen),
xiaowei.huang@liverpool.ac.uk (Xiaowei Huang), jimin.xiao@xjtlu.edu.cn (Jimin Xiao),
fei.ma@xjtlu.edu.cn (Fei Ma), szjsjt_oyrr@163.com (Renrong Ouyang)

developed an end-to-end single-stage framework without CAM, which improved training efficiency. Experimental results demonstrate that our method performs exceptionally well on public datasets, outperforming other state-of-the-art WSSS methods with a shorter training time.

Keywords: Weakly Supervised Learning, Semantic Segmentation, Contrastive Learning, Vision Transformer

1. Introduction

Semantic segmentation Yudin et al. (2024); Wang et al. (2023); Zhang et al. (2021a) is an important task in the field of computer vision Yin et al. (2023); Jiang et al. (2024); Li et al. (2024); Guo et al. (2024); Yin et al. (2024b,a). Weakly Supervised Semantic Segmentation (WSSS) is a continuously evolving approach in this field, which aims to generate pixel-level labels by utilizing weak supervision signals to significantly reduce the cost of annotations. Classic weak supervision signals include image-level labels Ahn & Kwak (2018); Jang et al. (2023); Xu et al. (2024); Zhang et al. (2024), points Bearman et al. (2016), scribbles Zhang et al. (2021b), and bounding boxes Lee et al. (2021b). Among the various weak supervision signals, most recent research has focused on the image-level label, primarily because it is the cheapest and contains the least information. This work also falls within the domain of WSSS, where it exclusively utilizes image-level labels.

Prevalent works of WSSS approaches relying on image-level class labels typically generate pseudo labels using class activation maps (CAM) Zhou et al. (2016). However, CAMs have limitations in accurately estimating both the shape and localization of objects belonging to the classes of interest Chen et al. (2022b). This has prompted researchers to incorporate additional refinements between the initial pseudo labels and the final pseudo labels generation. These refinements often involve multi-stage architectures, as observed in PAMR Araslanov & Roth (2020), thereby increasing complexity. Notable refinement strategies have been described in IRNet Ahn et al. (2019) and AdvCAM Lee et al. (2021a). How-

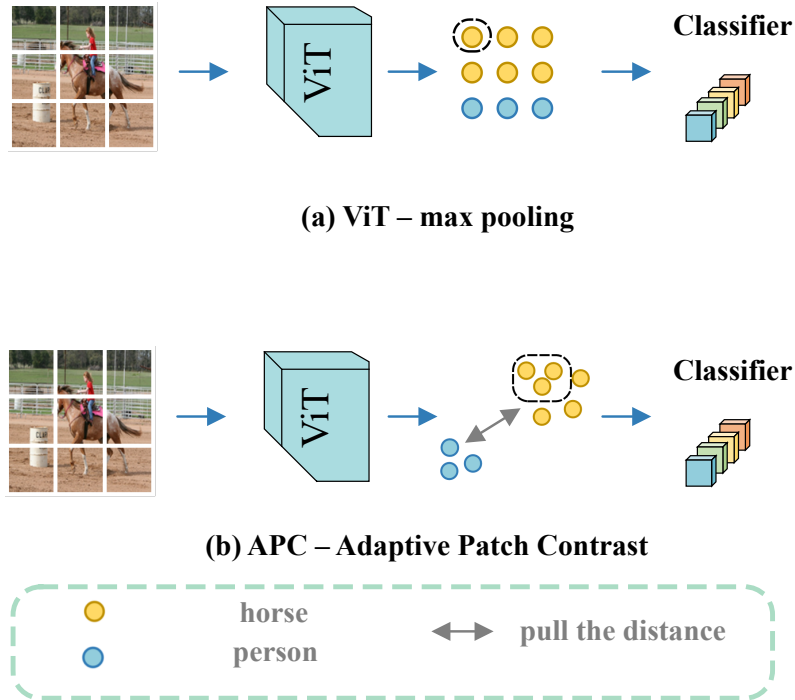


Figure 1: In the case of predicting the specific category 'horse': (a) Previous ViT-based method Dosovitskiy et al. (2020) uses the highest-scoring patch. (b) Our APC uses adaptive K patches and patch contrastive learning to enhance patch embeddings for image-level classification.

ever, these multi-stage architectures greatly impact computational performance, leading to inefficient training. In recent years, due to the limitations of CAM, researchers have turned to leverage ViT-based frameworks for WSSS Rossetti et al. (2022); Ru et al. (2023); Xu et al. (2022); Ru et al. (2022). ViT-PCM Rossetti et al. (2022) utilizes patch embeddings to infer the probability of pixel-level labels. Methods such as Ru et al. (2023); Xu et al. (2022) use ViT to replace CNN, thereby enhancing CAM's capability in object recognition. Additionally, AFA Ru et al. (2022) proposes an end-to-end architecture based on CAM and suggests acquiring reliable semantic affinity through attention blocks to enhance the initial coarse labels. However, current ViT-based methods utilize global max pooling to select the patch with the highest prediction score, projecting

patch-level classification to image-level, which may impact final performance due to misclassification. Moreover, frameworks without CAM are still in multi-stage training, requiring the separate generation of initial pseudo labels before proceeding to the next stage of training, which lacks efficiency

In this work, we empirically observe that existing ViT frameworks without CAM utilize a max pooling layer to connect image embedding patches with softmax, representing the probabilities of different image categories. However, max pooling has limitations as it may be dominated by individual outlier patches, lacking robustness. Therefore, we propose an effective approach called *Adaptive K pooling with patch contrastive learning*, as illustrated in Figure 1, to address the aforementioned issue. Firstly, we propose an Adaptive-K Pooling (AKP) module to overcome the limitations of max pooling by replacing it with a adaptive-k pooling layer. This helps in mitigating the influence of outlier patches and better represents the contribution of multiple different regions of objects to the final prediction. Specifically, in the AKP module, the original max pooling is replaced with a top-K pooling layer, where an adaptive algorithm based on numerical differences selects the optimal K value, addressing the issue of single-point dependence. Furthermore, to effectively combat the issue of over-smoothing, we propose a Patch Contrastive Learning (PCL) module to enhance intra-class compactness and inter-class separability, thereby generating more accurate patch predictions. In the PCL module, we calculate pairwise cosine similarities for patch embeddings generated by ViT, bringing closer the distances in the embedding space for the same category and increasing the distances between different classes, effectively improving the final performance. Building on the proposed AKP and PCL modules, we develop an end-to-end, single-stage WSSS framework without CAM, achieving notable improvements in computational efficiency.

Overall, the contributions of our work can be summarized as follows:

- 1) We propose Adaptive K Pooling (AKP) to address the limitation of segmentation performance being dominated by individual patches. The AKP method mitigates the influence of outlier patches and better represents the contribution of multiple different regions of objects to the final prediction.

2) We propose a patch-based contrastive learning module, in which we introduce the Patch Contrastive Learning (PCL). By computing the cosine similarity between patch pairs, we aim to increase the distance between patch pairs of different classes and reduce the distance between patch pairs of the same class, thereby enhancing the intra-class compactness and inter-class separability of patch embeddings and further improving the quality of pseudo labels.

3) We propose an end-to-end single-stage training framework based on ViT without CAM. This framework effectively enhances the training efficiency of WSSS. The Experiments on the PASCAL VOC 2012 Everingham et al. (2010) and MS COCO 2014 datasets Lin et al. (2014) show that the proposed APC outperforms other state-of-the-art WSSS methods with a shorter training time.

The remainder of this paper is organized into the following sections: Section 2 provides a summary of the related work, while Section 3 presents the proposed method. Section 4 details the experimental dataset, environmental setup, and outcomes. Finally, the conclusion, limitations of our work, and future directions are elaborated in Section 5.

2. Related work

2.1. WSSS with Image-level Labels

Existing WSSS methods commonly rely on image-level class labels as the cheapest form of supervision. Approaches using image-level class labels have traditionally been based on CAM methods Zhou et al. (2016), employing a standard multi-label classification network. The CAMs are derived by applying global average pooling (GAP) to the feature maps of the last layer, followed by concatenation into a weights vector. This vector is then connected to the class prediction through Binary Cross-Entropy (BCE) prediction loss. A common limitation of CAM is its tendency to activate only the most discriminative object regions. To address this limitation, recent studies have proposed various training strategies, including techniques such as erasing Wei et al. (2017), online attention accumulation Jiang et al. (2019), and cross-image semantic mining Sun et al.

(2020). Researchers in Chang et al. (2020) suggest leveraging auxiliary tasks to regularize the training objective, such as learning visual words. Contrast pixel and prototype representations Chen et al. (2022a); Du et al. (2022) to promote the comprehensive activation of object regions. To enable the network to capture more object parts, researchers have introduced greater challenges to the classification objective. This has been achieved by modifying either the input data Singh & Lee (2017); Wei et al. (2017); Wu et al. (2024); Zhang et al. (2021c); Li et al. (2018) or the feature maps Lee et al. (2019); Hou et al. (2018); Choe & Shim (2019), employing techniques like dropping out parts of the image or introducing perturbations. Some studies Chang et al. (2020) have made the classification task more difficult by adding finer-grained categories. Additionally, information across multiple images has been used to improve CAM maps Fan et al. (2020); Sun et al. (2020).

Typically, the limitation of these methods stems from their dependence on the CAM framework, which focuses primarily on the most discriminative object regions. To address this, we propose a novel WSSS framework that operates without CAM. We utilize Vision Transformer (ViT) to generate image patch embeddings and then utilize Adaptive K pooling to predict the categories of each patch. Finally, we map the patches to pixels as the segmentation result to address the limitation of CAM activating only the most discriminative object regions.

2.2. Vision Transformers for WSSS

Vision Transformer (ViT) Dosovitskiy et al. (2020) has achieved notable success across a range of vision tasks Carion et al. (2020); Dosovitskiy et al. (2020). This success has led to the adoption of ViT in Weakly Supervised Semantic Segmentation (WSSS), where ViT-based methods have begun to emerge as alternatives to traditional CNN-based approaches for generating Class Activation Maps (CAMs) Xu et al. (2022); Ru et al. (2022). Among these methods are models like MCTformer Xu et al. (2022) and AFA Ru et al. (2022), which, despite leveraging the strengths of ViT, still rely on CAMs. They utilize ViT’s

multi-head self-attention to capture global contextual information and employ an affinity module to propagate pseudo-masks. However, these approaches continue to face the inherent challenge of over-smoothing in ViT. ViT-PCM Rossetti et al. (2022) moves away from the reliance on CAMs by employing patch embeddings and max pooling to infer pixel-level label probabilities. This represents a notable advancement, as it is the first framework in WSSS that does not depend on CAMs to generate baseline pseudo-masks. Nonetheless, its reliance on max pooling introduces potential issues, particularly when patches are misclassified. This highlights a critical limitation in existing approaches, where either architectural adjustments or additional modules are required to mitigate the drawbacks of over-smoothing and misclassification.

In contrast to these methods, our approach employs ViT as the backbone and incorporates adaptive K pooling for the first time. This innovation addresses the limitations associated with max pooling and the potential for misclassification of patches within a framework that does not rely on CAM. Additionally, we introduce the Patch-level Contrastive Learning (PCL) module, which enhances intra-class compactness and inter-class separability of patch embeddings. This further improves the quality of the final labels, providing a more robust and accurate framework for WSSS without relying on CAMs.

2.3. Single-stage WSSS methods

Single-stage WSSS methods unify multiple stages such as classification, pseudo-label refinement, and segmentation into a single joint training process, greatly enhancing training efficiency compared to the previous multi-stage frameworks. 1Stage Araslanov & Roth (2020) achieves performance comparable to mainstream multi-stage methods by ensuring local consistency, semantic fidelity, and mask completeness. AFA Ru et al. (2022) explores the intrinsic architecture of ViT and extracts reliable semantic affinity from multi-head self-attention for pseudo-label refinement. ToCo Ru et al. (2023) addresses the observed issue of excessive smoothing in ViT by supervising the final patch tokens with intermediate knowledge. These works have pioneered effective single-stage, end-to-end

frameworks, offering a more concise and efficient paradigm for WSSS tasks. However, previous single-stage frameworks are fundamentally built upon CAM as a core component, limiting their potential due to CAM’s inherent drawback of activating only the most discriminative object regions. In contrast to these single-stage methods, we propose a novel framework that eliminates the reliance on CAM. By employing patch-level predictions directly to pixels, our approach overcomes the limitations of CAM-based methods and achieves state-of-the-art performance in WSSS.

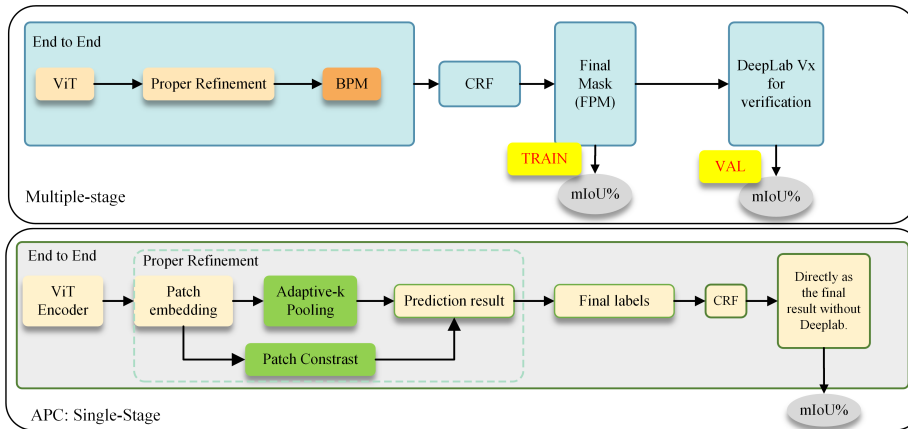


Figure 2: This figure compares the basic structure of a multiple-stage WSSS method (light blue) with our APC method (light gray). APC, based on the ViT framework without CAM, allows for a single-stage approach, enabling direct final label acquisition for verification without an additional semantic segmentation model (e.g., DeepLab Chen et al. (2017)).

3. Method

In this section, we introduce the overall structure and key components of our proposed method. Initially, in Section 3.1, we provide an overview of the APC method and compare it with the existing multi-stage approaches. Subsequently, in Section 3.2, we detail the specifics of our model framework, including how to obtain image patch embeddings from images and how to perform segmentation tasks. We have enhanced the existing non-CAM multi-stage framework into

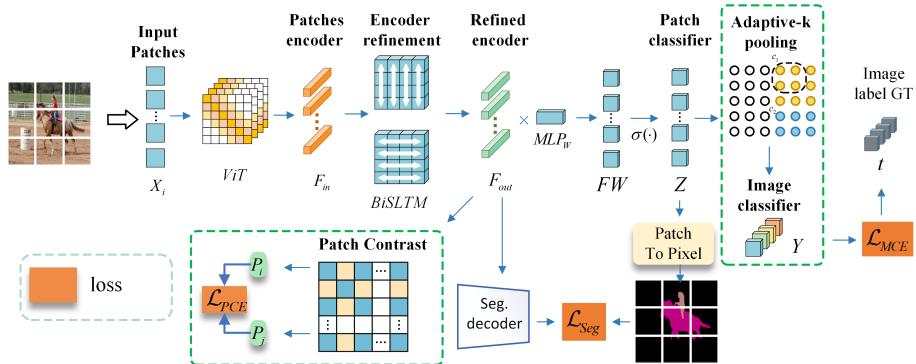


Figure 3: APC infrastructure: ViT encodes patch embeddings, which are refined by BiSLTM. MLP and softmax produce patch-to-classifier predictions. The AKP module maps patch classifiers to an image classifier using image-level ground truth for supervision. After the Refined Encoder, the PCL module enhances patch similarity.

a single-stage framework, incorporating a segmentation decoder that utilizes a decoder head to merge multi-level feature maps for prediction, implemented through simple MLP layers. In Section 3.3, we describe the proposed adaptive K pooling layer, which selects the final prediction patches by choosing different K values based on the ratio of prediction scores, aiming to address incorrect predictions dominated by a single patch. Furthermore, in Section 3.4, we discuss the integration of contrastive learning into our current framework. We introduce patch-level contrastive learning, calculating the cosine similarity for pairs of patch embeddings produced by ViT. We define patch contrastive learning (PCL) to enhance patch representations, reduce the distance between patches of the same category, and increase the distance between patches of different categories, thereby further improving prediction accuracy. Finally, in Section 3.5, we will summarize our APC overall loss.

3.1. Overall Framework

Our proposed APC method mainly consists of three main components: the adaptive K pooling module, the image patch contrastive module, and the end-

to-end encoder and decoder module, as illustrated in Figure 2. We first compare with the previous without CAM multiple-stage framework, where our significant improvement lies in transforming the entire WSSS process into a single stage. By introducing the encoder and decoder modules, we enable the framework to directly predict segmentation results during training. Next, we delve into the main proper refinement component of APC. In the first stage, the input image is divided into fixed-size patches, and then a ViT encoder is used to generate an embedding for each patch. Each patch here is represented as an embedding space vector. To further enhance the performance of the patch classifier, adaptive K pooling is employed for patch selection specific to certain categories, and these selected patches are then used for prediction. Additionally, we introduce the patch contrastive module, which adjusts the cosine similarity of patch embeddings belonging to the same categories to be closer and that of patch embeddings belonging to different categories to be farther apart. Through the aforementioned modules, our method obtains prediction results, which are directly used as final labels. After refinement with the Conditional Random Field (CRF) Krähenbühl & Koltun (2011), which is trained on PascalVOC in a fully supervised manner and introduced to WSSS by Kolesnikov & Lampert (2016), the results are directly used as the final output for verification, eliminating the need for an additional DeepLab stage.

3.2. Model Structure

This section provides a comprehensive explanation regarding the generation of patch embeddings and the design of the end-to-end single-stage WSSS task. The illustration of details about this method is shown in Figure 3. The input image $X_{in} \in \mathbb{R}^{h \times w \times 3}$ is firstly divided into s fixed-size input patches $X_{patch} \in \mathbb{R}^{d \times d \times 3}$, where $s = \frac{hw}{d^2}$. Then, the input patches X_{patch} are passed into ViT-based encoder to generate the patch embeddings $F_{in} \in \mathbb{R}^{s \times e}$. Next, HV-BiLSTM is used to enhance the representation of F_{in} and output refined patch embeddings F_{out} with the same size as F_{in} . Given the refined patch embedding F_{out} , we use a weight $W \in \mathbb{R}^{e \times |C|}$ and a softmax activation function to predict the class $c \in C$

of each patch in Eq. 1, where $|\mathcal{C}|$ is the total number of classes:

$$Z = \text{softmax}(F_{out}W). \quad (1)$$

The output $Z \in \mathbb{R}^{s \times |\mathcal{C}|}$ represents the prediction scores of each class for each patch. To robustly project from patch-level predictions to image-level predictions, we propose an adaptive K pooling module, described in Sec.3.3. The adaptive K module selects the top k patches $\{\bar{Z}_{i=1:k}^c\}$ with the highest value in each category and computes the average value as the prediction score for image-level classification in Eq. 2:

$$y_c = \frac{1}{k} \sum_{i=1}^k \bar{Z}_i^c, \quad (2)$$

where y_c is the projected image-level prediction score of class c . Adaptive K pooling ensures the final image prediction results are not dominated by any misclassified patches, thereby further improving the mapping from patch-level prediction to image-level prediction. We compute the distance between each patch pair using cosine similarity on the patch embeddings after refinement, and then apply contrastive learning, detailed in Section 3.4. Simultaneously, we introduce a decoder head to merge multi-level feature patch embeddings for prediction, implemented through a simple MLP layer. The decoder’s prediction is combined with our patch prediction category result to calculate the segmentation loss L_{seg} , where the predicted category of each patch is directly mapped onto each pixel within the patch as the pixel’s category for calculating the segmentation loss. For the segmentation loss L_{seg} , we utilize the commonly used cross-entropy loss. As illustrated in Figure 3, the supervision for the segmentation branch is the label refined through the Patch to Pixel module.

Finally, we minimize the error between the predicted image labels y_c and ground-truth labels t_c by using the multi-label classification prediction error

(MCE) in Eq. 3:

$$\begin{aligned} \mathcal{L}_{MCE} &= \frac{1}{|\mathcal{C}|} \sum_{c \in \mathcal{C}} BCE(t_c, y_c) \\ &= -\frac{1}{|\mathcal{C}|} \sum_{c \in \mathcal{C}} t_c \log(y_c) + (1 - t_c) \log(1 - y_c). \end{aligned} \tag{3}$$

We use binary labels and C independent Bernoulli distributions to model multi-label classification. With C representing the number of classes, C binary cross-entropy losses (BCE) measure the dissimilarity between predicted and ground-truth labels.

3.3. Patch Embeddings with Adaptive K Pooling

The motivation behind using Adaptive K pooling is to facilitate the mapping between patch-level classification and image-level classification. In previous work Rossetti et al. (2022), Global Max Pooling (GMP) only selects the patches with the highest prediction scores for each class, which may result in inaccurate mapping of patch-level predictions to image-level classification. In our experiments, we observed that some patches are misclassified with high prediction scores, and when there are multiple objects of the same categories in an image, a single patch as a prediction score may not effectively represent the overall mapping of the image to these categories. Therefore, to achieve a more robust mapping between patch-level and image-level classification, we average the prediction scores of the top k patches in each category as the prediction score for image-level classification. Additionally, we propose an adaptive algorithm to automatically select the value of k based on different scenarios, instead of using a fixed value of k . This allows for more flexible adaptation to various scenarios.

The illustration of details about this method is shown in Figure 3. The output $Z \in \mathbb{R}^{s \times |\mathcal{C}|}$ represents the prediction scores for each class for each patch. We replace the original max pooling layer with an adaptive K pooling layer to map the patch category predictions of the entire image to image category predictions. Regarding the selection of K, we propose an adaptive K pooling module, described in Algorithm 1. We use an adaptive algorithm to select k

patches as candidates for pooling. Specifically, we first sort the patch prediction scores for a given category c_i from high to low. Then, we select patches with sufficiently high scores as candidates to ensure that we can optimize not only the region corresponding to the patch with the highest score but also multiple regions with high scores.

Algorithm 1: Adaptive K selection

Input: $input_tensor$ of patch-to-categories prediction scores, number of categories C

Output: $AdaptiveK_candidate$ after adaptive K selection

```

1  $AdaptiveK\_candidate \leftarrow \emptyset$ 
2 foreach category  $c_i$  in  $C$  do
3    $selected\_elements \leftarrow$  top-1 values of  $input\_tensor$  for category  $c_i$ 
4   for  $i \leftarrow 2$  to  $K$  do
5      $current\_elements \leftarrow$  top- $i$  values of  $input\_tensor$  for category  $c_i$ 
6      $mean\_current \leftarrow$  compute mean of  $current\_elements$ 
7      $mean\_selected \leftarrow$  compute mean of  $selected\_elements$ 
8     if  $\frac{mean\_current}{mean\_selected} > \theta$  then
9        $selected\_elements \leftarrow current\_elements$ 
10   $AdaptiveK\_candidate[c_i] \leftarrow selected\_elements$ 
11 return  $AdaptiveK\_candidate$ 

```

In our observation, we found that for each patch generating predictions for a specific category Z , in images containing multiple objects, besides the patch with the maximum prediction score, patches with prediction scores close to the maximum score also represent the category well. We designed an adaptive algorithm that automatically expands the selected set when it detects patches with prediction scores close to the maximum score and the difference between them is less than θ .

3.4. Patch Contrastive Learning

To enhance the representation of patch embeddings and thus improve the accuracy of prediction, the patch contrastive learning (PCL) is used to narrow the distance between patch embeddings with high prediction scores in a specific category c and also expand the distance between patch embeddings with high scores and the low confidence patch embeddings in the same category. In this work, cosine similarity is used to measure the distance between patch embeddings in Eq. 4:

$$S(F_{out}^i, F_{out}^j) = \frac{F_{out}^i \cdot F_{out}^j}{\|F_{out}^i\| \|F_{out}^j\|}, \quad (4)$$

where a higher similarity value means two patch embeddings are closer to each other, and a lower value indicates a further distance. To represent the similarity more explicitly, as shown in Eq. 5, we normalize the range of value between 0 and 1 via:

$$\bar{S}(F_{out}^i, F_{out}^j) = \frac{1 + S(F_{out}^i, F_{out}^j)}{2}. \quad (5)$$

As illustrated in Figure 3, F_{out} is used as the input of PCL module. Furthermore, the patch prediction score Z_i^c and a threshold ϵ are used to determine whether a patch is a high confidence one $\mathcal{P}_{high}^c = \{F_{out}^i | Z_i^c > \epsilon\}$. Similarly, the patch with the lowest prediction score is considered as a low confidence one $\mathcal{P}_{low}^c = \{F_{out}^i | Z_i^c < (1 - \epsilon)\}$. Then, in Eq. 6, the patch contrastive learning error (PCE) of a category c can be expressed as:

$$\begin{aligned} \mathcal{L}_{PCE}^c &= \frac{1}{N_{pair}^+} \sum_{i=1}^{|\mathcal{P}_{high}^c|} \sum_{j=1, j \neq i}^{|\mathcal{P}_{high}^c|} (1 - \bar{S}(F_{high}^i, F_{high}^j)) \\ &+ \frac{1}{N_{pair}^-} \sum_{m=1}^{|\mathcal{P}_{high}^c|} \sum_{n=1}^{|\mathcal{P}_{low}^c|} \bar{S}(F_{high}^m, F_{low}^n), \end{aligned} \quad (6)$$

where N_{pair}^+ denotes the number of pairs of patches with high confidence, N_{pair}^- denotes the number of pairs of high confidence and low confidence patches. F_{high}

and F_{low} represent the feature embeddings of high confidence patch \mathcal{P}_{high}^c and low confidence patch \mathcal{P}_{low}^c , respectively.

3.5. Overall loss

As illustrated in Figure 3, we have introduced multiple losses in the previous sections, including the contrastive learning L_{pce} loss, the classification L_{mce} loss, and the segmentation loss L_{seg} . The overall loss of our APC, as shown in Eq. 7, is the weighted sum of L_{pce} , L_{mce} , and L_{seg} :

$$\mathcal{L} = \mathcal{L}_{mce} + \lambda_1 \mathcal{L}_{seg} + \lambda_2 \sum_{c \in \mathcal{C}} \mathcal{L}_{PCE}^c, \quad (7)$$

where λ_1 , and λ_2 balance the contributions of different losses.

4. Experiments

In this section, we describe the experimental settings, including dataset, evaluation metrics, and implementation details. We then compare our method with state-of-the-art approaches on PASCAL VOC 2012 dataset Everingham et al. (2010) and MS COCO 2014 Lin et al. (2014). Finally, ablation studies are performed to validate the effectiveness of crucial components in our proposed method.

Table 1: **Impact of Image Size in the Inference Stage:** Performance is evaluated on the VOC val set. The default settings are highlighted in gray as the baseline.

Size	Seg.	Inference Time (seconds)	Memory (GB)
640 ²	71.6	369	11.1
800 ²	72.1	426	11.9
960 ²	72.3	483	13.7
1120 ²	72.0	920	18.8

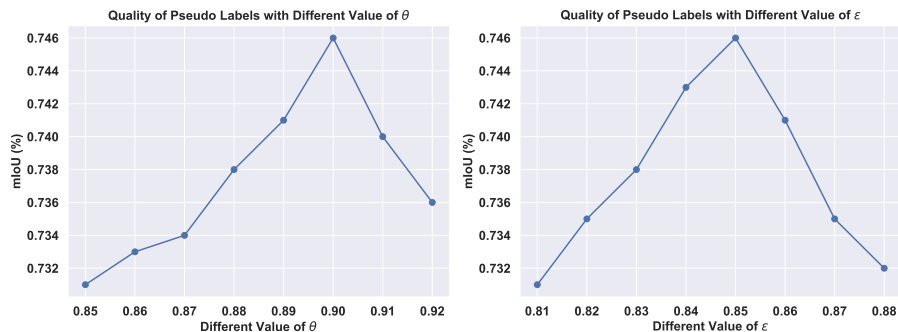


Figure 4: The performance comparison of selecting different values of θ and ϵ .

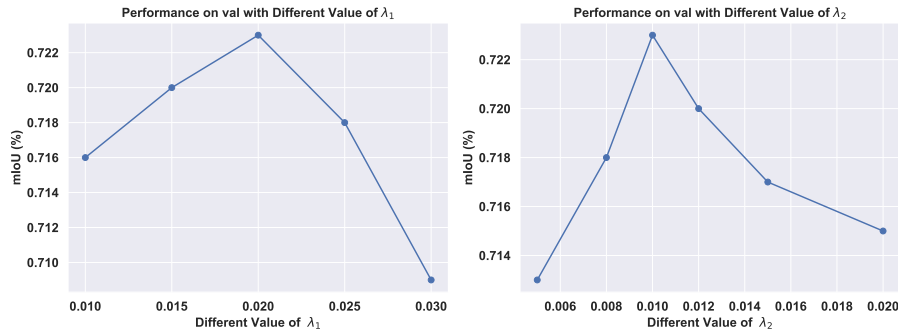


Figure 5: The performance comparison of selecting different values of λ_1 and λ_2 .

4.1. Experimental Settings

Dataset and Evaluated Metric. Our experiments are conducted on two benchmark datasets: PASCAL VOC 2012 Everingham et al. (2010), which includes 21 classes, and MS COCO 2014 Lin et al. (2014), featuring 81 classes. Each dataset also contains an extra class for background. The PASCAL VOC 2012 dataset is commonly expanded using the SBD dataset Hariharan et al. (2011). For training on PASCAL VOC 2012, we use 10,582 images with image-level labels and 1,449 images for the validation set. In the case of the MS COCO 2014 dataset, approximately 82k images are used for training and around 40k images for validation, with the training images having only image-level annotations. The performance is evaluated using the mean Intersection-Over-Union (mIoU) metric.

Table 2: Results of predicted pseudo masks on PASCAL VOC 2012 train.

Method	Pub.	Backbone	mIoU (%)
SEAM Wang et al. (2020)	CVPR20	V1-RN38	63.6
CONTA Zhang et al. (2020)	NeurIPS20	V1-RN38	67.9
CDA Su et al. (2021)	ICCV21	V1-RN38	66.4
EPS Lee et al. (2021c)	CVPR21	V2-RN101	71.4
Yao <i>et al.</i> Yao et al. (2021)	CVPR21	V2-RN101	68.3
AuxSegNet Xu et al. (2021)	ICCV21	V1-RN38	69.0
AdvCAM Lee et al. (2022)	PAMI22	V2-RN101	69.9
PPC Du et al. (2022)	CVPR22	ResNet38	61.5
SIPE Chen et al. (2022a)	CVPR22	ResNet50	58.6
AFA Ru et al. (2022)	CVPR22	MiT-B1	66.0
ViT-PCM Dosovitskiy et al. (2020)	ECCV22	ViT-B/16	71.4
ToCo Ru et al. (2023)	CVPR23	ViT-B/16	72.2
USAGE Peng et al. (2023)	ICCV23	ResNet38	72.8
FPR Chen et al. (2023)	ICCV23	ResNet38	68.5
APC (Ours)		ViT-B/16	74.6

Our APC approach demonstrates substantial improvements in segmentation results on both PASCAL VOC 2012 and MS COCO 2014 datasets.

Implementation Details. In our experiments, we utilize the ViT-B/16 model as the backbone for the ViT encoder. During the training process, input images are initially resized to 384×384 , as suggested in Kolesnikov et al. (2016) Kolesnikov & Lampert (2016), and subsequently partitioned into 24×24 small patches for the ViT encoder. For the inference stage, we resize the image to 960×960 and the impact of image size is assessed on the VOC val set, with default settings indicated in baseline color gray, as illustrated in Table 1. We observe that the increase in memory usage from 640 to 800 is relatively small, rising from 11.1 GB to 11.9 GB. This may be attributed to

the intermediate layers not reaching their memory bottleneck and the GPU’s effective memory compression or optimization. However, when increasing from 960 to 1120, memory usage jumps from 13.7 GB to 18.8 GB, accompanied by a drop in performance. Building on insights from prior work Kabir & Garg (2023); Bolon-Canedo & Remeseiro (2020), we learn that higher data complexity does not necessarily lead to better results. In fact, reducing the complexity from 1120 to 960 not only decreases data complexity but also improves overall performance. The model is trained with a batch size of 16 and for a maximum of 15 epochs, utilizing two NVIDIA 4090 GPUs. We employ the Adam optimizer and schedule the learning rate as follows: the learning rate is set to 10^{-3} for the first two epochs, and then to 10^{-4} for the remaining epochs. We set the threshold ϵ to 0.85 to determine high-confidence patches in PCE, and k is set to 6 for adaptive-K pooling. The default weight coefficients λ_1 and λ_2 are set to 0.02 and 0.01, respectively, as shown in Figure 5. We employed grid search to determine the optimal values for λ_1 and λ_2 within specified ranges. Initially, we removed the λ_2 module and enumerated possible values for λ_1 within $[0, 1]$, adjusting the step size from larger to smaller increments until we identified the optimal value for λ_1 . We then followed a similar approach for λ_2 . This stepwise adjustment aimed to isolate the effect of each parameter on model performance. Finally, we applied the learned values of λ_1 and λ_2 to the MS COCO dataset, where we observed SOTA results as well. And θ is set to 0.9. As shown in Figure 4, the performance is compared by selecting different values for θ and ϵ . During the validation phase, we do not require additional DeepLab training for full supervision. Instead, we directly use the model’s prediction results as the final labels and validate them on the validation set.

4.2. Comparisons with State-of-the-art

Comparison of Pseudo Masks. We evaluated the performance of our APC method on the PASCAL VOC 2012 dataset for pseudo mask prediction, using 10,582 images with only image-level labels to train the segmentation network. Subsequently, we conducted segmentation predictions on these 10,582

Table 3: Final Semantic segmentation performance for training on Pascal VOC 2012 val.

Model	Pub.	Backbone	mIoU (%)
<i>Multiple-Stage method</i>			
MCTformer Xu et al. (2022)	CVPR22	DeiT-S	61.7
SIPE Chen et al. (2022a)	CVPR22	ResNet50	58.6
ViT-PCM Dosovitskiy et al. (2020)	ECCV22	ViT-B/16	69.3
USAGE Peng et al. (2023)	ICCV23	ResNet38	71.9
SAS Kim et al. (2023)	AAAI23	ViT-B/16	69.5
FPR Chen et al. (2023)	ICCV23	ResNet38	70.0
<i>End-To-End Single-Stage</i>			
AFA Ru et al. (2022)	CVPR22	MiT-B1	63.8
ToCo Ru et al. (2023)	CVPR23	ViT-B/16	70.5
TSCD Xu et al. (2023)	AAAI23	MiT-B1	67.3
APC (End-To-End)		ViT-B/16	72.3

images. As demonstrated in Table 2, our APC method outperforms other state-of-the-art techniques, encompassing both multi-stage and single-stage approaches, by achieving an mIoU value of 74.6% on the training data. This achievement is credited to our proposed adaptive-K pooling method, which dynamically selects an optimal number of K patches for category prediction scores, effectively addressing the challenge of mapping patch-level classification to image-level classification using a single patch’s prediction score. Additionally, the incorporation of patch contrastive learning further boosts the overall performance.

Comparison of Segmentation Results. In this study, we compared the final segmentation performance of our proposed APC end-to-end method on the PASCAL VOC 2012 and MS COCO 2014 datasets. As shown in Table 3, consistent with other comparative methods, we utilized 10,582 images with only image-level labels as the training set to train our APC model. For validation, we

Table 4: Final Semantic segmentation performance for training on MS COCO 2014 val set.

Model	Pub.	Backbone	mIoU (%)
<i>Multiple-Stage method</i>			
MCTformer Xu et al. (2022)	CVPR22	Resnet38	42.0
ViT-PCM Dosovitskiy et al. (2020)	ECCV22	ViT-B/16	45.0
SIPE Chen et al. (2022a)	CVPR22	Resnet38	43.6
OCR Cheng et al. (2023)	CVPR23	ViT-B/16	42.5
SAS Kim et al. (2023)	AAAI23	ViT-B/16	44.8
FPR Chen et al. (2023)	ICCV23	ResNet38	43.9
<i>End-To-End Single-Stage</i>			
AFA Ru et al. (2022)	CVPR22	MiT-B1	38.9
ToCo Ru et al. (2023)	CVPR23	ViT-B/16	42.3
TSCD Xu et al. (2023)	AAAI23	MiT-B1	40.1
APC (Ours)		ViT-B/16	45.7

employed 1,449 images to assess our final semantic segmentation performance, where our end-to-end single-stage method outperformed both recent end-to-end approaches and multiple-stage methods. Notably, the end-to-end method significantly surpasses multiple-stage methods in computational efficiency, offering substantial savings in capacity. These details will be further elaborated in Section 4.3. Regarding the MS COCO 2014 dataset, we adopted a similar approach, using approximately 82k images for training and around 40k images for validation to evaluate the final semantic segmentation performance. As indicated in Table 4, our method continued to exhibit superior performance.

4.3. Ablation Studies

Performance and Computational Efficiency. Table 5 demonstrates the superiority of our APC in terms of computational performance. We conducted ablation experiments comparing the baseline ViT-based end-to-end single-stage

Table 5: Ablation studies on computational efficiency and final performance for Pascal VOC 2012 and MS COCO 2014 datasets.

Dataset	Baseline (ViT-B)	AKP	PCL	Time (Hours)	mIoU (%)
VOC	✓			4±1	68.2
VOC	✓	✓		3±0.5	70.3
VOC	✓	✓	✓	1.5±0.5	72.3
COCO	✓			9±2	42.8
COCO	✓	✓		7±1	44.2
COCO	✓	✓	✓	3±1	45.7

Table 6: Efficiency performance of APC compared to others on Pascal VOC 2012 validation set.

Method	Time (Hours)	Val (%)
Multiple-Stage Methods		
ViT-PCM Rossetti et al. (2022)	8±1	69.3
End-to-End Methods		
AFA Ru et al. (2022)	2.5±0.5	63.8
ToCo Ru et al. (2023)	2±0.5	70.5
APC (Ours)	1.5±0.5	72.3

module (without AKP and PCL), the Adaptive-K Pooling (AKP) module, and the Patch Contrastive Learning (PCL) module. Based on findings from prior research Ru et al. (2022, 2023), traditional multi-stage methods are less efficient than end-to-end approaches. This is because multi-stage methods typically involve training pseudo-labels in the first stage, followed by their use as training data for fully supervised Deeplab network training, which consumes significant computational resources. Therefore, we also include a comparison with other end-to-end methods in Table 6 to evaluate the runtime performance of our approach. To ensure fairness in experimentation, all comparisons were conducted

on a single NVIDIA 4090 GPU machine. As shown in Table 5, In Pascal VOC 2012, our baseline ViT-based end-to-end single-stage module required 4 hours to complete. Incorporating the Adaptive-K Pooling (AKP) module further reduced the runtime to approximately 3 hours. Finally, with the addition of contrastive learning, significant performance improvements were observed, with the model typically converging within 15 epochs. The total training time was reduced to approximately 1.5 hours. The same benefits are observed in alignment with the results on MS COCO 2014. The Experimental results demonstrate that our approach not only greatly enhances the final segmentation performance but also significantly improves computational efficiency, thereby conserving more computational resources.

Table 7: Ablation studies on different pooling strategies and keeping other components consistent for final semantic segmentation performance on Pascal VOC 2012 val.

Average pooling	Max-Pooling	Top-K	AKP	mIoU(%)
✓				61.7%
	✓			70.5%
		✓		71.8%
			✓	72.3%

Table 8: Ablation studies on our APC model for the final semantic segmentation performance on the Pascal VOC 2012 val. The components constitute the initial baseline.

Backbone (ViT)	HV-BiLSTM	CRF	AKP	PCL	Seg mIoU (%)
✓					62.6%
✓	✓				65.3%
✓	✓	✓			68.6%
✓	✓	✓	✓		70.3%
✓	✓	✓	✓	✓	72.3%

The Impact of Different Pooling Strategies. Table 7 presents ablation

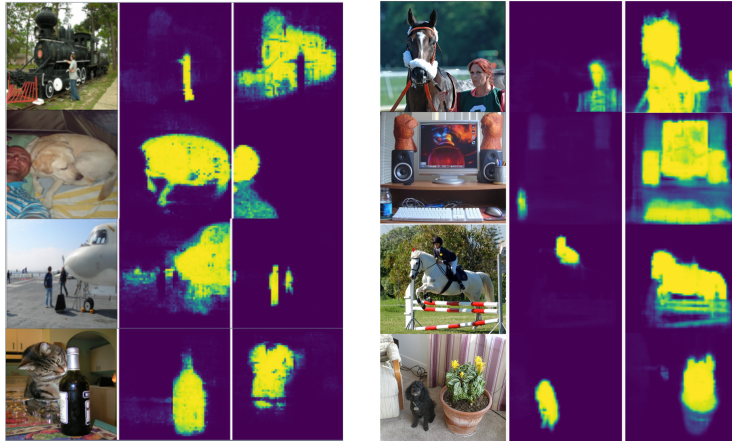


Figure 6: The sample illustrates probabilities highlighted by 60×60 heatmaps, which are generated from the patch to pixel module to produce pixel probabilities.

studies on various pooling strategies for final semantic segmentation performance. We compared the performance of average pooling layer, max pooling layer, fixed top-K pooling layer, and our proposed adaptive-K pooling layer. To ensure fair experimentation, we incorporated the PCL module and utilized an end-to-end framework in all cases. The only difference lies in the choice of pooling layer. The experiments were conducted on the Pascal VOC 2012 validation dataset. We observed that our proposed adaptive-K pooling achieved the highest performance.

Table 9: Comparison of Inter-Class and Intra-Class Cosine Distances With and Without PCL.

Method	Type	Cosine Distance
With PCL	Inter-class	0.9556
With PCL	Intra-class	0.5664
Without PCL	Inter-class	0.9473
Without PCL	Intra-class	0.7152

The Impact of Different component. The ablation studies of different components in our framework are presented in Table 8. We designed the experiments to analyze the impact of HV-BiLSTM, CRF, AKP, and PCL.



Figure 7: The comparison of qualitative segmentation results from top to bottom: the images, GT, max-pooling (ViT-PCM Dosovitskiy et al. (2020)), ViT+AKP, and our APC utilizing ViT+AKP+PCL.

HV-BiLSTM and CRF serve as our baselines, marked in gray, as both are well-established methods from previous research with proven effectiveness for WSSS tasks. Our key contributions, AKP and PCL, are shown in Table 8, AKP improves the final segmentation performance by 1.7% mIoU compared to max pooling. Additionally, by incorporating the proposed PCL, which applies contrastive learning at the patch level within each image, enhancing inter-class separability and improving intra-class consistency in the feature space, the segmentation task performance was further improved by 2.0% mIoU. Meanwhile, we design a new metric to measure inter-class separability using cosine distance based on category embeddings. Specifically, we use patch embeddings from the intermediate results of our model, similar to the cosine distance in the PCL method. As shown in Table 9, we observe that after applying PCL, the inter-class distance increases, while the intra-class distance decreases compared to before. This result verifies that our PCL module enhances inter-class separability and improves intra-class consistency. Therefore, these two components significantly

contribute to outperforming previous ViT-based methods in our approach.

4.4. Visualization Results

Visualization of Heatmaps. We present the results of heatmap visualization in Figure 6, where probabilities are highlighted by 60×60 heatmaps. Pixels with values in yellow indicate the probability of belonging to the predicted class. Through the heatmap results, we can see that in key areas of the object, the probabilities are high, while they gradually decrease at the edges. Our APC effectively segments the objects.

Segmentation Visualization Results. We present the final semantic segmentation results in Figure 7. Additionally, we compared these results with those of the previous max-pooling-based method, demonstrating a significant improvement in semantic segmentation performance. Specifically, we observe that in the results from max-pooling, the segmentation regions are highly concentrated. This is due to max-pooling being limited to the areas surrounding individual patches. For instance, in human segmentation, max-pooling tends to focus on regions around the face, such as the eyes and nose, while neglecting areas like the hair. With our AKP module, however, the segmentation of the person is significantly enhanced. Regarding the PCL module, we observe substantial improvements in object boundary segmentation. By leveraging inter-class and intra-class contrastive learning, PCL effectively enhances the segmentation of object edges.

5. Conclusion

In this work, we propose APC approach without using CAM for weakly supervised semantic segmentation. Unlike previous methods, APC utilizes adaptive-K pooling to select k patches for mapping patch-level classification to image-level classification, thus mitigating the issue of potential misclassified patches. In addition, patch contrastive learning (PCL) is proposed to further enhance the feature embeddings of patches. In the same class, PCL aims to

decrease the distance between patch embeddings with high confidence and increase the distance between embeddings with high confidence and embeddings with low confidence. By combining these two components, our method achieves state-of-the-art results in weakly supervised semantic segmentation tasks using only image-level labels.

However, a limitation of our framework is that it relies solely on image information as input. In WSSS tasks, the category information for each image is typically available. If this information were incorporated as text and fused with image features through multimodal integration, it could potentially enhance segmentation performance, particularly in accurately identifying object boundaries. In comparison, our current approach depends exclusively on image data, which may not offer the most optimal solution.

In future work, we will further enhance segmentation performance by enriching the input information with semantic features and integrating category text features into the images for model training. However, the current network architecture presents challenges for directly utilizing text features in a multimodal fusion approach. Therefore, future studies should consider designing a network model that can effectively accommodate both text and image inputs.

References

- Ahn, J., Cho, S., & Kwak, S. (2019). Weakly supervised learning of instance segmentation with inter-pixel relations. In *Proc. IEEE Conf. Comput. Vis. Pattern Recog.* (pp. 2209–2218).
- Ahn, J., & Kwak, S. (2018). Learning pixel-level semantic affinity with image-level supervision for weakly supervised semantic segmentation. In *Proc. IEEE Conf. Comput. Vis. Pattern Recog.* (pp. 4981–4990).
- Araslanov, N., & Roth, S. (2020). Single-stage semantic segmentation from image labels. In *Proc. IEEE Conf. Comput. Vis. Pattern Recog.* (pp. 4253–4262).

- Bearman, A., Russakovsky, O., Ferrari, V., & Fei-Fei, L. (2016). What’s the point: Semantic segmentation with point supervision. In *Eur. Conf. Comput. Vis.* (pp. 549–565). Springer.
- Bolon-Canedo, V., & Remeseiro, B. (2020). Feature selection in image analysis: a survey. *Artificial Intelligence Review*, *53*, 2905–2931.
- Carion, N., Massa, F., Synnaeve, G., Usunier, N., Kirillov, A., & Zagoruyko, S. (2020). End-to-end object detection with transformers. In *Eur. Conf. Comput. Vis.* (pp. 213–229). Springer.
- Chang, Y.-T., Wang, Q., Hung, W.-C., Piramuthu, R., Tsai, Y.-H., & Yang, M.-H. (2020). Weakly-supervised semantic segmentation via sub-category exploration. In *Proc. IEEE Conf. Comput. Vis. Pattern Recog.* (pp. 8991–9000).
- Chen, L., Lei, C., Li, R., Li, S., Zhang, Z., & Zhang, L. (2023). Fpr: False positive rectification for weakly supervised semantic segmentation. In *Proc. IEEE Int. Conf. Comput. Vis.* (pp. 1108–1118).
- Chen, L.-C., Papandreou, G., Kokkinos, I., Murphy, K., & Yuille, A. L. (2017). Deeplab: Semantic image segmentation with deep convolutional nets, atrous convolution, and fully connected crfs. *IEEE Trans. Pattern Anal. Mach. Intell.*, *40*, 834–848.
- Chen, Q., Yang, L., Lai, J.-H., & Xie, X. (2022a). Self-supervised image-specific prototype exploration for weakly supervised semantic segmentation. In *Proc. IEEE Conf. Comput. Vis. Pattern Recog.* (pp. 4288–4298).
- Chen, Z., Wang, T., Wu, X., Hua, X.-S., Zhang, H., & Sun, Q. (2022b). Class re-activation maps for weakly-supervised semantic segmentation. In *Proc. IEEE Conf. Comput. Vis. Pattern Recog.* (pp. 969–978).
- Cheng, Z., Qiao, P., Li, K., Li, S., Wei, P., Ji, X., Yuan, L., Liu, C., & Chen, J. (2023). Out-of-candidate rectification for weakly supervised semantic

- segmentation. In *Proc. IEEE Conf. Comput. Vis. Pattern Recog.* (pp. 23673–23684).
- Choe, J., & Shim, H. (2019). Attention-based dropout layer for weakly supervised object localization. In *Proc. IEEE Conf. Comput. Vis. Pattern Recog.*
- Dosovitskiy, A., Beyer, L., Kolesnikov, A., Weissenborn, D., Zhai, X., Unterthiner, T., Dehghani, M., Minderer, M., Heigold, G., Gelly, S. et al. (2020). An image is worth 16x16 words: Transformers for image recognition at scale. *arXiv preprint arXiv:2010.11929*, .
- Du, Y., Fu, Z., Liu, Q., & Wang, Y. (2022). Weakly supervised semantic segmentation by pixel-to-prototype contrast. In *Proc. IEEE Conf. Comput. Vis. Pattern Recog.* (pp. 4320–4329).
- Everingham, M., Van Gool, L., Williams, C. K., Winn, J., & Zisserman, A. (2010). The pascal visual object classes (VOC) challenge. *Int. J. Comput. Vis.*, *88*, 303–338.
- Fan, J., Zhang, Z., Tan, T., Song, C., & Xiao, J. (2020). Cian: Cross-image affinity net for weakly supervised semantic segmentation. In *AAAI Conf. Artif. Intell.* (pp. 10762–10769). volume 34.
- Guo, X., Chen, X., Luo, S., Wang, S., & Pun, C.-M. (2024). Dual-hybrid attention network for specular highlight removal. In *ACM MM* (pp. 10173–10181).
- Hariharan, B., Arbeláez, P., Bourdev, L., Maji, S., & Malik, J. (2011). Semantic contours from inverse detectors. In *Proc. IEEE Int. Conf. Comput. Vis.* (pp. 991–998).
- Hou, Q., Jiang, P., Wei, Y., & Cheng, M.-M. (2018). Self-erasing network for integral object attention. In *Int. Conf. Neur. Info. Process. Sys.* (pp. 547–557).
- Jang, S., Kwon, J., Jin, K., & Kim, Y. (2023). Weakly supervised semantic segmentation via graph recalibration with scaling weight unit. *Engineering Applications of Artificial Intelligence*, *119*, 105706.

- Jiang, P.-T., Hou, Q., Cao, Y., Cheng, M.-M., Wei, Y., & Xiong, H.-K. (2019). Integral object mining via online attention accumulation. In *Proceedings of the IEEE/CVF international conference on computer vision* (pp. 2070–2079).
- Jiang, Y., Chen, X., Pun, C.-M., Wang, S., & Feng, W. (2024). Mfdnet: Multi-frequency deflare network for efficient nighttime flare removal. *The Visual Computer*, (pp. 1–14).
- Kabir, H., & Garg, N. (2023). Machine learning enabled orthogonal camera goniometry for accurate and robust contact angle measurements. *Scientific reports*, *13*, 1497.
- Kim, S., Park, D., & Shim, B. (2023). Semantic-aware superpixel for weakly supervised semantic segmentation. In *AAAI Conf. Artif. Intell.* (pp. 1142–1150). volume 37.
- Kolesnikov, A., & Lampert, C. H. (2016). Seed, expand and constrain: Three principles for weakly-supervised image segmentation. In *Eur. Conf. Comput. Vis.* (pp. 695–711).
- Krähenbühl, P., & Koltun, V. (2011). Efficient inference in fully connected crfs with gaussian edge potentials. *Advances in neural information processing systems*, *24*.
- Lee, J., Kim, E., Lee, S., Lee, J., & Yoon, S. (2019). Ficklenet: Weakly and semi-supervised segmentation using stochastic inference. In *Proc. IEEE Conf. Comput. Vis. Pattern Recog.* (pp. 5267–5276).
- Lee, J., Kim, E., Mok, J., & Yoon, S. (2022). Anti-adversarially manipulated attributions for weakly supervised semantic segmentation and object localization. *IEEE Trans. Pattern Anal. Mach. Intell.*, .
- Lee, J., Kim, E., & Yoon, S. (2021a). Anti-adversarially manipulated attributions for weakly and semi-supervised semantic segmentation. In *Proc. IEEE Conf. Comput. Vis. Pattern Recog.* (pp. 4071–4080).

- Lee, J., Yi, J., Shin, C., & Yoon, S. (2021b). Bbam: Bounding box attribution map for weakly supervised semantic and instance segmentation. In *Proc. IEEE Conf. Comput. Vis. Pattern Recog.* (pp. 2643–2652).
- Lee, S., Lee, M., Lee, J., & Shim, H. (2021c). Railroad is not a train: Saliency as pseudo-pixel supervision for weakly supervised semantic segmentation. In *Proc. IEEE Conf. Comput. Vis. Pattern Recog.* (pp. 5495–5505).
- Li, K., Wu, Z., Peng, K.-C., Ernst, J., & Fu, Y. (2018). Tell me where to look: Guided attention inference network. In *Proc. IEEE Conf. Comput. Vis. Pattern Recog.* (pp. 9215–9223).
- Li, M., Sun, H., Lei, Y., Zhang, X., Dong, Y., Zhou, Y., Li, Z., & Chen, X. (2024). High-fidelity document stain removal via a large-scale real-world dataset and a memory-augmented transformer. In *WACV*.
- Lin, T.-Y., Maire, M., Belongie, S., Hays, J., Perona, P., Ramanan, D., Dollár, P., & Zitnick, C. L. (2014). Microsoft coco: Common objects in context. In *Eur. Conf. Comput. Vis.* (pp. 740–755). Springer.
- Peng, Z., Wang, G., Xie, L., Jiang, D., Shen, W., & Tian, Q. (2023). Usage: A unified seed area generation paradigm for weakly supervised semantic segmentation. In *Proc. IEEE Int. Conf. Comput. Vis.* (pp. 624–634).
- Rossetti, S., Zappia, D., Sanzari, M., Schaerf, M., & Pirri, F. (2022). Max pooling with vision transformers reconciles class and shape in weakly supervised semantic segmentation. In *Eur. Conf. Comput. Vis.* (pp. 446–463).
- Ru, L., Zhan, Y., Yu, B., & Du, B. (2022). Learning affinity from attention: End-to-end weakly-supervised semantic segmentation with transformers. In *Proc. IEEE Conf. Comput. Vis. Pattern Recog.* (pp. 16846–16855).
- Ru, L., Zheng, H., Zhan, Y., & Du, B. (2023). Token contrast for weakly-supervised semantic segmentation. In *Proc. IEEE Conf. Comput. Vis. Pattern Recog.* (pp. 3093–3102).

- Singh, K. K., & Lee, Y. J. (2017). Hide-and-seek: Forcing a network to be meticulous for weakly-supervised object and action localization. In *Proc. IEEE Int. Conf. Comput. Vis.*.
- Su, Y., Sun, R., Lin, G., & Wu, Q. (2021). Context decoupling augmentation for weakly supervised semantic segmentation. In *Proc. IEEE Int. Conf. Comput. Vis.* (pp. 7004–7014).
- Sun, G., Wang, W., Dai, J., & Van Gool, L. (2020). Mining cross-image semantics for weakly supervised semantic segmentation. In *Computer Vision–ECCV 2020: 16th European Conference, Glasgow, UK, August 23–28, 2020, Proceedings, Part II 16* (pp. 347–365). Springer.
- Wang, H., Cao, G., & Cao, W. (2023). A novel inference paradigm based on multi-view prototypes for one-shot semantic segmentation. *Applied Intelligence*, .
- Wang, Y., Zhang, J., Kan, M., Shan, S., & Chen, X. (2020). Self-supervised equivariant attention mechanism for weakly supervised semantic segmentation. In *Proc. IEEE Conf. Comput. Vis. Pattern Recog.* (pp. 12275–12284).
- Wei, Y., Feng, J., Liang, X., Cheng, M.-M., Zhao, Y., & Yan, S. (2017). Object region mining with adversarial erasing: A simple classification to semantic segmentation approach. In *Proc. IEEE Conf. Comput. Vis. Pattern Recog.* (pp. 1568–1576).
- Wu, W., Dai, T., Huang, X., Ma, F., & Xiao, J. (2024). Image augmentation with controlled diffusion for weakly-supervised semantic segmentation. In *IEEE Int. Conf. Acoust. Speech Signal Process.*.
- Xu, L., Bennamoun, M., Boussaid, F., Laga, H., Ouyang, W., & Xu, D. (2024). Mctformer+: Multi-class token transformer for weakly supervised semantic segmentation. *IEEE transactions on pattern analysis and machine intelligence*, .

- Xu, L., Ouyang, W., Bennamoun, M., Boussaid, F., Sohel, F., & Xu, D. (2021). Leveraging auxiliary tasks with affinity learning for weakly supervised semantic segmentation. In *Proc. IEEE Int. Conf. Comput. Vis.* (pp. 6984–6993).
- Xu, L., Ouyang, W., Bennamoun, M., Boussaid, F., & Xu, D. (2022). Multi-class token transformer for weakly supervised semantic segmentation. In *Proc. IEEE Conf. Comput. Vis. Pattern Recog.* (pp. 4310–4319).
- Xu, R., Wang, C., Sun, J., Xu, S., Meng, W., & Zhang, X. (2023). Self correspondence distillation for end-to-end weakly-supervised semantic segmentation. In *AAAI Conf. Artif. Intell.* (pp. 3045–3053). volume 37.
- Yao, Y., Chen, T., Xie, G.-S., Zhang, C., Shen, F., Wu, Q., Tang, Z., & Zhang, J. (2021). Non-salient region object mining for weakly supervised semantic segmentation. In *Proc. IEEE Conf. Comput. Vis. Pattern Recog.* (pp. 2623–2632).
- Yin, J., Peng, N., Chen, Y., Zheng, Z., Gu, Y., & Zhou, J. (2024a). Class-level multiple distributions representation are necessary for semantic segmentation. In *International Conference on Database Systems for Advanced Applications* (pp. 340–351). Springer.
- Yin, J., Yan, S., Chen, T., Chen, Y., & Yao, Y. (2024b). Class probability space regularization for semi-supervised semantic segmentation. *Computer Vision and Image Understanding*, 249, 104146.
- Yin, J., Zheng, Z., Pan, Y., Gu, Y., & Chen, Y. (2023). Semi-supervised semantic segmentation with multi-reliability and multi-level feature augmentation. *Expert Systems with Applications*, 233, 120973.
- Yudin, D., Zakharenko, N., Smetanin, A., Filonov, R., Kichik, M., Kuznetsov, V., Larichev, D., Gudov, E., Budenny, S., & Panov, A. (2024). Hierarchical waste detection with weakly supervised segmentation in images from recycling plants. *Engineering Applications of Artificial Intelligence*, 128, 107542.

- Zhang, B., Xiao, J., Jiao, J., Wei, Y., & Zhao, Y. (2021a). Affinity attention graph neural network for weakly supervised semantic segmentation. *IEEE Transactions on Pattern Analysis and Machine Intelligence*, *44*, 8082–8096.
- Zhang, B., Xiao, J., & Zhao, Y. (2021b). Dynamic feature regularized loss for weakly supervised semantic segmentation. *arXiv preprint arXiv:2108.01296*, .
- Zhang, D., Zhang, H., Tang, J., Hua, X., & Sun, Q. (2020). Causal intervention for weakly-supervised semantic segmentation. In *Int. Conf. Neur. Info. Process. Sys.* (pp. 655–666). volume 33.
- Zhang, F., Gu, C., Zhang, C., & Dai, Y. (2021c). Complementary patch for weakly supervised semantic segmentation. In *Proc. IEEE Int. Conf. Comput. Vis.* (pp. 7242–7251).
- Zhang, J., Peng, B., Wu, X., & Hu, J. (2024). Weakly supervised semantic segmentation by knowledge graph inference. *Engineering Applications of Artificial Intelligence*, *138*, 109294.
- Zhou, B., Khosla, A., Lapedriza, A., Oliva, A., & Torralba, A. (2016). Learning deep features for discriminative localization. In *Proc. IEEE Conf. Comput. Vis. Pattern Recog.* (pp. 2921–2929).